Materials Research Express

PAPER

Investigation of self-consistent site-dependent DFT + U effect on electronic band structure and optical properties of $SiFe_2O_4$ spinel

M C Idris[1,2], A Shaari[1], R Razali[1], Abdullahi Lawal[1,3] and S T Ahams[1,4]

[1] Physics Department, Universiti Teknologi Malaysia, 81310 Skudai Johor, Malaysia
[2] Physics Department, Sule Lamido University Kafin-Hausa, Jigawa State, Nigeria
[3] Physics Department, Federal College of Education Zaria, Kaduna State. Nigeria
[4] Physics Department, Adamawa State University Mubi, Nigeria

E-mail: idrischiromawa@graduate.utm.my

Keywords: optoelectronics properties, $SiFe_2O_4$ spinel, DFT + U, dielectric constants, random phase approximation

OPEN ACCESS

RECEIVED
27 November 2019

REVISED
29 January 2020

ACCEPTED FOR PUBLICATION
13 February 2020

PUBLISHED
24 February 2020

Abstract

The first-principle investigation of $SiFe_2O_4$ (SFO) spinel was performed with the help of a plane-wave pseudopotential technique within the generalized gradient approximation (GGA) and local density approximation (LDA) as implemented in Quantum Espresso Simulation package. The Electronic band structure and optical properties of SFO spinel-type material have been investigated and discussed in this paper. The calculated band structure reveals that SFO spinel-type material is a direct bandgap semiconductor. Using GGA + U and LDA + U the band gap value so obtained is 3.52 eV and 2.96 eV respectively. The contribution to valence and conduction bands due to different bands was analyzed on the basis of the total and partial density of state. The Optical properties of SFO spinel-type material have been calculated and discussed in detail. The real, $\varepsilon_1(\omega)$ and the imaginary, $\varepsilon_2(\omega)$ part of the complex dielectric constants is found to be 6.52 and 5.42 at energies of 3.44 eV and 6.21 eV respectively. The refractive index $n(0)$ and the reflectivity index ($R(\omega)$), at zero energy value were found to be 1.88 and 10% respectively. We found that SFO spinel-type material has good properties for optical devices.

1. Introduction

Transparent conducting oxides (TCOs) are materials that are characterized by high electrical conductivity charge concentration and simultaneously very high optical transparency to visible light [1]. In 1907 the first report of TCOs (Cadmium Oxide, CdO) was published by Badekar [2], who used thermal oxidation of sputtered films of cadmium. From that time many researchers delve into the field of TCO so that new types of TCOs with broad range applications can be prepared. Some of the widely known used TCOs include In_2O_3: Sn (ITO), Sn_2O:F (FTO), ZnO:F (ZFO), as well as new TCOs in spinels, form such as; $MgIn_2O_4$, Zn Ga_2O_4, $ZnRh_2O_4$, Zn_2TiO_4 [1, 3–5].

Spinel-type transition-metal oxides encompass a group of compounds having a general chemical formula of XM_2O_4, with M and X cations occupying two nonequivalent lattice sites: one with six octahedrally (O_h) coordinated oxygens and the other with four tetrahedrally (T_d) coordinated nearest-neighbor oxygen atoms [6]. Owing to the possibility of accommodating earths abundant transition metals in different oxidation states at the O_h and T_d sites, spinels such as the $CuFe_2O_4$, $GaZn_2O_4$, $CuCo_2O_4$ and $SnMg_2O_4$, offer an excellent opportunities for designing many technological applications which include: transparent conducting oxides (TCOs), [7–11], humidity sensors, magnetic materials for spintronics and storage devices, redox materials for solar-thermal water splitting, high surface-reactivity catalysts for water-gas shift reactions, electrodes in lithium-ion as well as sodium-ion batteries, and hydrogen generation for microbial systems [12–16]. In a 'normal' XM_2O_4 spinel-type oxide, all X cations occupy the O_h sites while the M cations occupy T_d sites, whereas, in an 'inverse' spinel-type, the O_h sites are shared equally by X and M cations with the T_d sites occupied only by X cations [17].

In the past few years, the use of first-principles methods to the study of compounds of geophysical interest has greatly expanded and even comprehensive studies of the thermodynamical properties of some spinels are made available [9, 14, 18]. At the same time, the treatment of iron-containing minerals bears additional difficulties due to the possible presence of strong electron- correlation effects. Of these spinel oxides, the spinel $SiFe_2O_4$ (SFO) is particularly attractive due to its earth's abundance as well as its robust physical and chemical properties. Although the SFO spinel-type had been studied experimentally by using different methods [19–21], yet, to the best of our knowledge, the theoretical information on the electronic properties of this important compound is narrowly reported [22, 23]. Consequently, In this paper, the electronic band properties, structure study and optical properties of the SFO spinel-type material are systematically investigated using the self-consistent (sc) calculations based on the first principle (DFT) method, where other information such as partial density of state (Pdos), band structure, Fermi energy, bandgap type, density of states (DOS), width of the conduction and valence bands, etc can be obtained from DFT calculations.

To overcome the problem of standard DFT on underestimation of the bandgap which can lead, in extreme cases, to incorrect calculations of a system as metallic rather than insulating, many theoretical techniques, like the quantum Monte Carlo (QMC) approaches, optimised effective potential (OEP) method, dynamical mean-field theory (DMFT). and DFT + U (GGA + U/LDA + U) methods (that are applied for the strongly correlated and localized 3*d* or 4*f* electrons in rare-earth and transition oxides), have been developed [24, 25]. For the purpose of this work, we employed the GGA + U and LDA + U techniques so that, the Fe 3d state is treated by using Hubbard extensions to approximate DFT energy functionals. This method will serve as a better choice and computationally less expensive for the correct prediction of fundamental energy bandgap closer to the experimental measurements. In addition, we investigated the optical properties of SFO spinel-type material via Random phase approximation (RPA) based on GGA + U + RPA.

Even though the electronic structure of solid-state materials at room temperature can be found from many experimental techniques as demonstrated by Ono and Zhang *et al* [26, 27] yet, it is anticipated that the DFT + U carried out in the present work, will provide more basic theoretical background and understandings of the ground and excited-state properties of the SFO spinel-type material.

2. Computational details

In the present calculations of the total energy and electronic band structure of SFO, we used plane wave self-consistent field (PWscf) code, distributed with the Quantum ESPRESSO (QE) simulation package [28] with ultrasoft pseudopotentials (USPPs). The exchange-correlation (XC) potential is approximated by Generalized Gradient Approximation (GGA), with Perdew–Burke–Ernzerhof (PBE) and Local Density Approximation (LDA) in the form of Perdew-Zunger (PZ) parameterization [29, 30]. the take into account, the on-site Coulomb interactions between 3d electrons, we used the value of the Coulomb integral $U = 5.3$ eV (following [31]) for Fe in the DFT + U calculations. The valance states of the atoms considered in the USPPs are as *follows:* Si:3 s,3p, Fe:3s,4s, 3p, 3d, and O:2 s, 2p state. An automatically generated 8 × 8 × 8 sampling k-point grid following the convention of Monkhorst and Pack [32] is used for Brillouin-Zone (BZ) integration yielding 721 k-points in the irreducible wedge of the BZ centered at Γ-point. The band structure calculations have been carried out following a path along the high symmetry points Γ-L-B_1/B-Z- Γ-X/Q-F-P_1-Z/L-P. The internal coordinates of these points are (0, 0, 0), (1/2, 0, 0), (1/2, 1/4, 1/4), (3/4, 1/2, 1/4), (1/2, 1/2, 1/2), (3/8, 0, −3/8), (5/8, 3/8, 0), (1/2, 1/2, 0), (5/8, 5/8, 1/4) and (3/4, 3/8, 3/8) in the first BZ, respectively as proposed by Wahyu and Stefanu [33]. Wave functions are expanded in plane-wave basis sets up to a kinetic energy cut-off value of 600 Ry.

All calculations were performed using the optimized structural parameters obtained in this work as shown in figure 1. We obtained equations of state (EOS's) for SFO using some volume points, fitted the total energies to the Birch-Murnaghan EOS [34], and derived the equilibrium energy and volumes, bulk modulus derivative (B′) and bulk moduli (B_0). Optical properties of SFO spinel-type material were performed using Yambo code at the level of GGA + U within random phase approximation. GGA + U is chosen because the bandgap obtained with it is closer to the experimental result [35–37]. The complex dielectric function $\varepsilon(\omega) = \varepsilon_1(\omega) + \varepsilon_2(\omega)$ is an important function that describes the optical properties of a material. Using equation (1) the real part ($\varepsilon_1(\omega)$) was calculated by employing the Kramers-Kronig relations while the imaginary part ($\varepsilon_2(\omega)$) of the complex dielectric function is obtained by summing transitions from valence (occupied) to conduction (unoccupied) states (with fixed k) over the BZ as shown in equation (2) [38].

$$\varepsilon_1(\omega) = 1 + \left(\frac{2}{\pi}\right) \mathrm{P} \int_0^{\infty} \frac{\omega' \int_{2(\omega)}}{(\omega'^2 - \omega^2)} \int \mathrm{d}\omega' \tag{1}$$

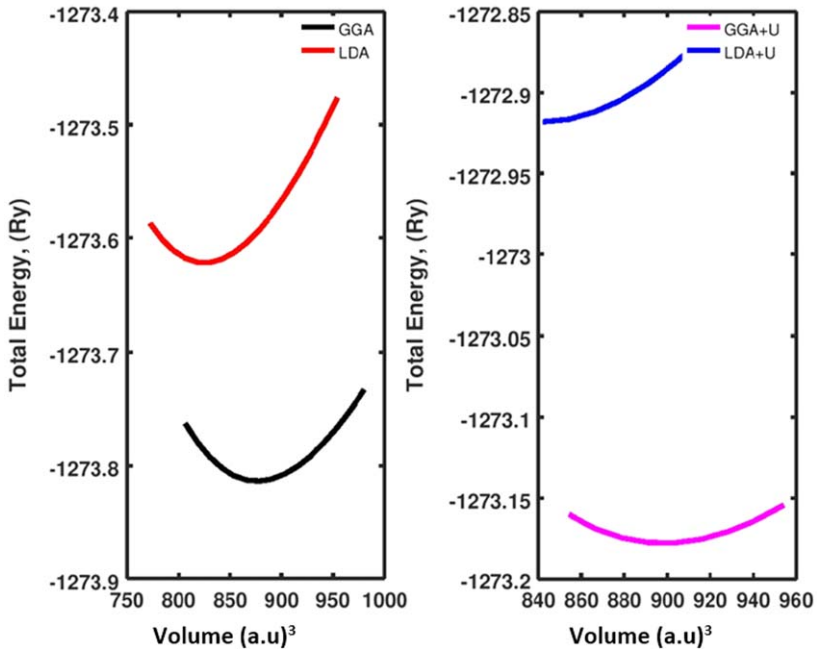

Figure 1. Structural Optimized Plots of the equilibrium total energies as a function of the unit cell volumes of the SFO spinel-type material.

$$\varepsilon_2(\omega) = \frac{4e^2\pi}{\omega^2 m^2}\left(\sum_{c,v}\int_k c_k\ |P|v_k\,^2\delta(\epsilon_{c_k} - \epsilon_{v_k} - \omega\hbar)\,dk\right) \tag{2}$$

where P represents the Cauchy principal value, c_k and v_k are the Bloch functions for the unoccupied and occupied states. The symbols ω and k denote the frequency of incident radiation and momentum operator respectively while the total energy is given by an integral part of equation (2).

The results obtained from equations (1) and (2) were used to calculate other frequency-dependent complex dielectric functions such as the extinction coefficient (k(ω)), conductivity (σ(ω)), reflectivity index (R(ω)), absorption coefficient (α(ω)), electron loss function (L(ω)) and the refractive index (n(ω)) as given in the equations (3)–(8) [38, 39].

$$k(\omega) = \sqrt{\frac{1}{2}}\ (-\varepsilon_1(\omega) + \sqrt{\varepsilon_1^2(\omega) + \varepsilon_2^2(\omega)})^{\frac{1}{2}} \tag{3}$$

$$\sigma(\omega) = \frac{1}{4\pi}\ (\omega\varepsilon_2(\omega)) \tag{4}$$

$$R(\omega) = \left(\frac{\sqrt{i\varepsilon_2(\omega) + \varepsilon_1(\omega) - 1}}{\sqrt{i\varepsilon_2(\omega) + \varepsilon_1(\omega) + 1}}\right)^2 \tag{5}$$

$$\alpha(\omega) = \left(\frac{\omega}{c}\right)(2(\varepsilon_2^2(\omega) + \varepsilon_1^2(\omega))^{\frac{1}{2}} - \varepsilon_1^2(\omega))^{\frac{1}{2}} \tag{6}$$

$$L(\omega) = \left(\frac{\varepsilon_2(\omega)}{\varepsilon_1^2(\omega) + \varepsilon_2^2(\omega)}\right) \tag{7}$$

$$n(\omega) = \sqrt{\frac{1}{2}}\ (\varepsilon_1(\omega) + (\varepsilon_1^2(\omega) + \varepsilon_2^2(\omega))^{\frac{1}{2}})^{\frac{1}{2}} \tag{8}$$

3. Results and discussion

3.1. Structure parameters

Firstly, in order to avoid certain errors and obtain correct results for electronic and optical properties, complete geometry optimization of the spinel structure for both lattice parameters and atomic coordinates is performed. The optimized structural cell parameters of the SFO are listed in table 1. The lattice parameter, a_0 of SFO and the total energy (lowest value of the parabolic energy-volume curves as illustrated in figures 1(a) and (b)) of the unit cell in the SFO spinel-type material are varied due to variation of volume, V_0 where, the calculated lattice

Table 1. Optimized Lattice parameters (a_0), Total Equilibrium Energy (E_0), volume (V_0), bulk moduli (B_0) and bulk modulus derivative (B') from Murnaghan's EOS.

Method	a_0 (a.u)	V_0 (a.u)^3	B_0 (GPa)	B'	E_0 (Ry)
GGA	5.683	876.22	235.7	4.37	−1273.812
LDA	5.563	825.80	221.3	4.42	−1273.622
GGA + U	5.736	896.03	275.3	4.34	−1273.178
LDA + U	5.583	836.91	263.7	4.11	−1272.919
Experiment (31)	5.895	920.868	181		
			168.9 [40]	5.7 [40]	

parameters and volumes when compared with experimental results show a small and consistent decrease (<11%), while values of B_0 and B' obtained from the EOS fitting show an underestimation of less than 10%. These deviations are due to the use of GGA/LDA in our DFT calculations and is a well-known consequence of, LDA calculations which underestimate the lattice parameters relative to the experimental values while GGA typically produce larger lattice parameters than the LDA, in some cases so much higher than they overestimate the lattice constants [24]. In this work, we observed that the use of GGA and LDA in our calculation miscalculate the lattice parameter by 4.85% and 10.32% respectively. However, incorporating the U scheme tends to decrease the error in the lattice parameter relative to bare GGA/LDA results. The calculated lattice parameter with the inclusion of the U corrections is interestingly close to the experimental results as shown in table 1. This confirmed that the inclusion of the U corrections in the DFT calculations of correlated and localized 3*d* or 4*f* electrons in rare-earth and transition oxides is significant for predicting reliable lattice parameters as it gives an excellent equivalent with experimental results.

3.2. Electronic properties

The calculated bands energy and total density of state (TDOS) structure curves of SFO are presented in figures 2(a)–(d) using the GGA/LDA and GGA + U/LDA + U. The electronic bands energy in figures 2(a) and (c) appear to illustrate no energy gap at the Fermi level, thus, standard DFT failed to predict the insulator properties of SFO spinel-type material despite the fact that, it was found to be an insulator experimentally. In order to understand the characteristics of electronic band states of SFO and to correct this problem, another approach is needed to be able to investigate the properties conscientiously. In this work, we have used DFT + U approximation to resolve the bandgap of SFO. The calculated bandgap based on DFT + U with different approximations is reported in table 2. Some of our results agreed well with that of the experiment. The detailed knowledge of the electronic structure of a material is important in assessing its potential applications in optical and optoelectronic devices. In figures 2 (b) and (d) the valance band maxima (VBM) and the conduction band minima (CBM) from both GGA + U and LDA + U lies at the same symmetry point F. This indicates that SFO has a direct energy bandgap. The calculated band gaps for the SFO material are 3.52 eV and 2.96 eV using GGA + U and LDA + U respectively. The bandgap obtained using the GGA + U is closer to the experimental value of 4.22 eV which was obtained using spectroscopic technique relative to LDA + U [41, 42]. The slight incongruities noted between the bandgap value obtained from GGA + U and the experimental is usually attributed to some physical aspects.

Firstly, the renowned limitation of the DFT is the use of approximations to treat the exchange-correlation energies in the DFT calculations (where the approximations do not fully replicate the exact exchange-correlation interactions in the compounds). Nevertheless, GW approximation has been employed for the subsequent calculations of the fundamental band gap and other optical properties of the material. The GW method has been repeatedly used by many researchers and provide an accurate description of the band gaps of semiconductors and insulators as well as reproducing the bandgap trends as reported in more complicated hybrid (exact) functional or computationally expensive methods [36, 37, 45]. Secondly, due to the pre-conditions adopted in the DFT formalism where the ground and excited states properties calculations of the materials are performed at temperature, $\theta = 0\ K$, and this, is much lower than the temperatures at which the experimental properties of many materials were measured [46].

Consequently, this may perhaps lead to additional discrepancies that are observed between the DFT calculated and the experimental band gap values of SFO as depicted in figures 2(b) and (d). It is worthy to note that, the calculated energy band gaps of the studied material (SFO) lie between 2.69 eV to 3.60 eV and this indicates that, SFO may be efficiently utilized as ideal transparent materials (TM) [1, 23].

The PDOS (partial density of states) for the Si, Fe, O atoms of the bulk SFO spinel-type material are investigated through the GGA + U and LDA + U as illustrated in figures 3(a) and (b). The PDOS plots in figure 3 clearly display that there is an energy range (below the fermi, E_F as well as above it) where the DOS

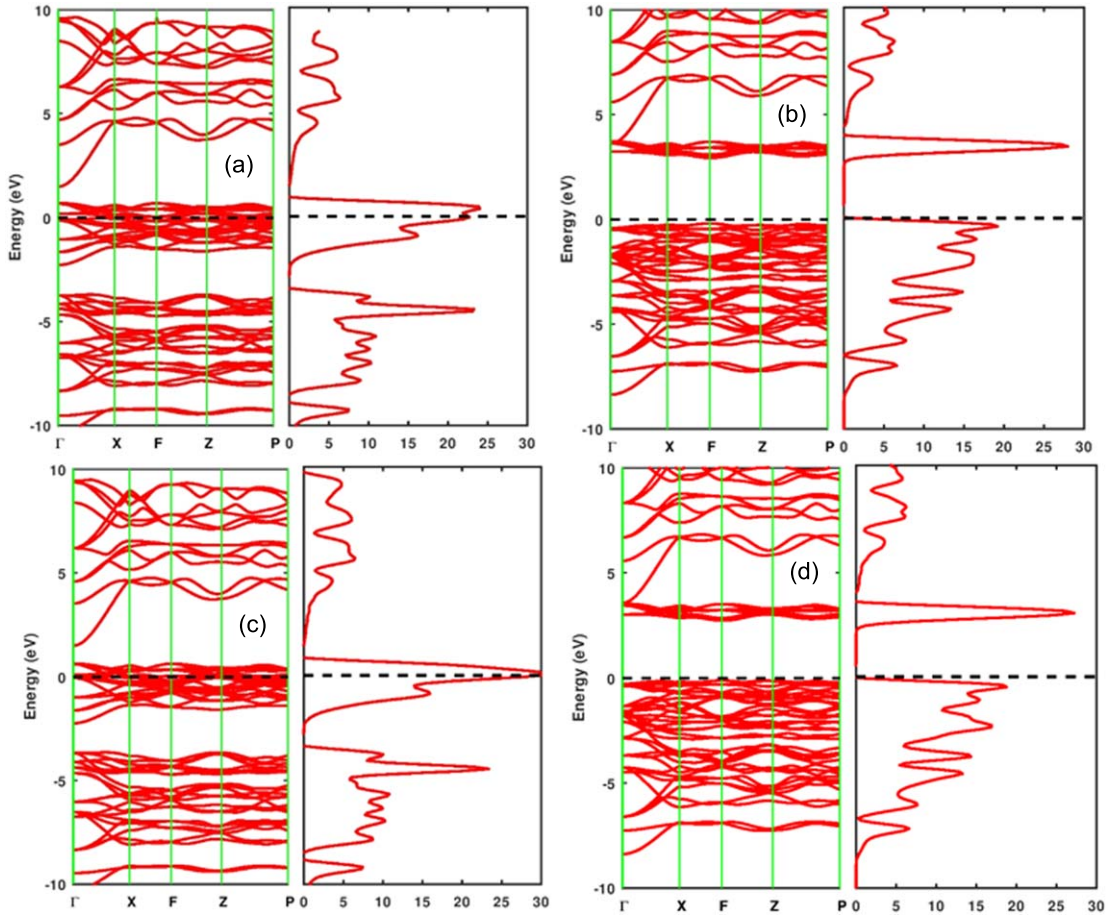

Figure 2. Calculated Bands Energy and TDOS: (a) GGA (b) GGA + U (c) LDA (d) LDA + U.

Table 2. Calculated Energy band gaps (in eV) of SFO Spinel-type Material.

	GGA + U	LDA + U
This work	3.52	2.96
Experiment	4.22 [41, 42]	
Others	2.21 [43], 2.52 [44], 1.49 [22]	

remains at zero, hence, confirming that the SFO spinel-type is an insulator [41]. Furthermore, the PDOS plots in figure 3 reveal two main regions one in the VB and the other in the CB of the SFO spinel-type using both GGA + U and LDA + U. The first region below fermi (−0.94 eV to −7.20 eV) consists of the contributions by the Fe-3d, O-2p, Si-3s and Fe-3p states using GGA + U while for LDA + U is from −0.55 eV to 8.15 eV which consist of Fe-3d, Si-3s, O-2p and O-2s states.

The conduction band region from (2.58 eV above fermi) is mainly contributed by the Fe-3d, O-2p, Fe-4s states using the GGA + U and that of LDA + U from 2.41 eV above the fermi consist of Si-3s, Fe-3d, O-2s and O-2p states. Notably, the mixed nature of the density of states suggests strong hybridization among the states of cations and anions. From figures 3(a) and (b), it can be clearly observed that there are significant contributions of the Si-3s and O-2s states in both GGA + U and LDA + U. Thus, the PDOS plots offer additional information such as the degree of the various contributions from the different states due to the different elements in the SFO spinel-type and this will complement the experimental results of this material that were previously reported.

3.3. Optical properties

As stated in equation (1), the complex dielectric function ($\varepsilon(\omega)$) shows the optical response of the material at all photon energies. The real part ($\varepsilon_1(\omega)$), of the dielectric function, gives the energy stored in material while the imaginary part ($\varepsilon_2(\omega)$) is connected to the absorption behavior of the medium together with the electronic band structure of the material. We have shown in figure 4 (a and b) how $\varepsilon_1(\omega)$ and $\varepsilon_2(\omega)$ of the complex dielectric

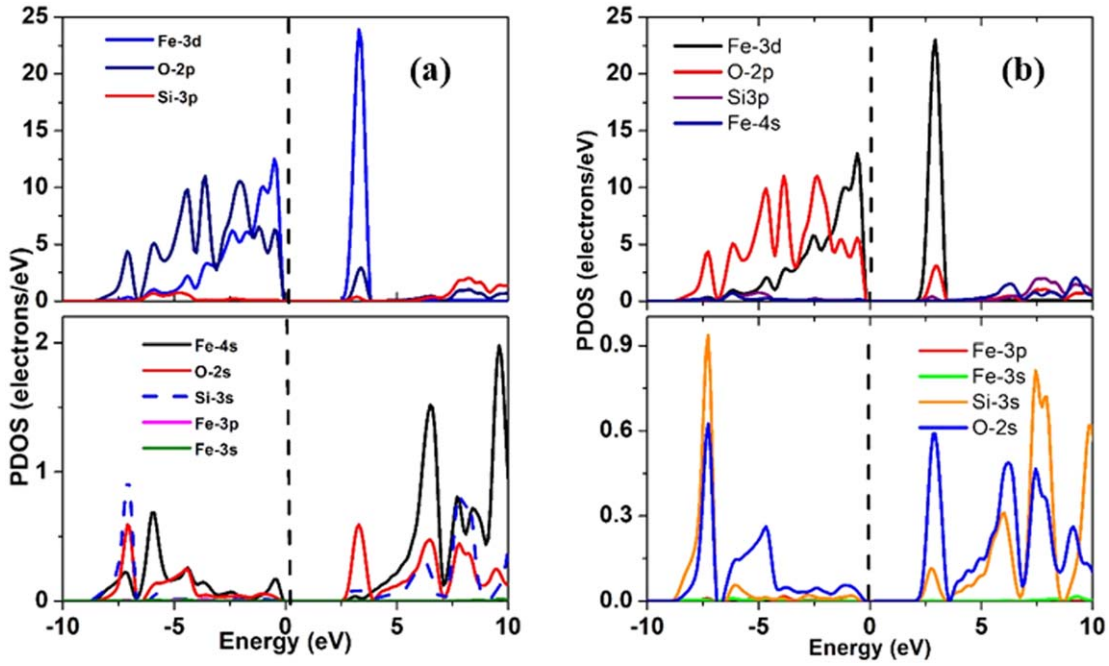

Figure 3. The calculated Partial Density of State (PDOS) for the Si, Fe, O atoms in the bulk SFO using (a) GGA + U and (b) LDA + U.

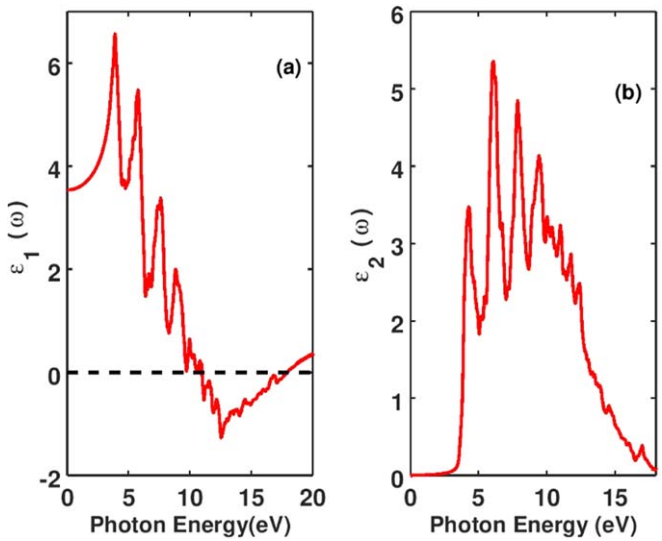

Figure 4. Calculated Complex Dielectric Plots of the (a) Real part (b) Imaginary part.

function of the SFO spinel-type varied with photon energy (E). The corresponding value $\varepsilon_1(0)$ at $\omega = 0$ for SFO spinel-type material is given in table 3. After $\omega = 0$ the magnitude of $\varepsilon_1(\omega)$ start to increase with increasing photon energy, and the values of $\varepsilon_1(\omega)$ where the peaks of the $\varepsilon_1(\omega)$ spectra occur and the corresponding values of the photon energy for the SFO spinel-type material are also listed in table 3.

Furthermore, within the energy range of 9.58–17.82 eV the spectra of $\varepsilon_1(\omega)$ is negative and this indicates that this material shows metallic behavior in this photon energy range, which becomes reflective towards the incoming photons. The plot of $\varepsilon_2(\omega)$ in figure 4(b) demonstrated the variation of the frequency-dependent absorptive part of the complex dielectric function with photon energy while the threshold energy of the $\varepsilon_2(\omega)$ spectra are also listed in table 3. The calculated $\varepsilon_2(\omega)$ show that the optical absorption edge occurred at 3.52 eV, which is sometimes called optical bandgap. This value corresponds to the energy bandgap of the material under investigation, which characterizes the interband transition between maxima of the valence band and minima of the conduction band. It is worthy to note that, the different peaks in figure 4(b) are as a result of the electronic interband transitions and the origin of the different peaks can be related to the partial density of state plots

Table 3. Calculated Static Parameters of the real part of the Complex Dielectric of the SFO Spinel-type.

Real part, $\varepsilon_1(\omega)$		Imaginary part, $\varepsilon_2(\omega)$	
$\varepsilon_1(0)$	3.53	$E^{Threshold}$(eV)	3.52
$\varepsilon_1^{min}(\omega)$	−1.56	$\varepsilon_2^{max}(\omega)$	5.42
E^{min}(eV)	1 2.52	E^{max}(eV)	6.21
$\varepsilon_1^{max}(\omega)$	6.52		
E^{max}(eV)	3.44		

The minimum and maximum values of the components of the complex dielectric ($\varepsilon_1^{min}(\omega)$, $\varepsilon_1^{max}(\omega)$, $\varepsilon_2^{min}(\omega)$, $\varepsilon_2^{max}(\omega)$) spectra and their corresponding values of energies E^{min}(eV), E^{max}(eV) at the point where the peaks occur. Also, the value of $\varepsilon_1(\omega)$ at the point where $E = 0$, as well as the threshold energy and its minimum negative value, are listed in the table.

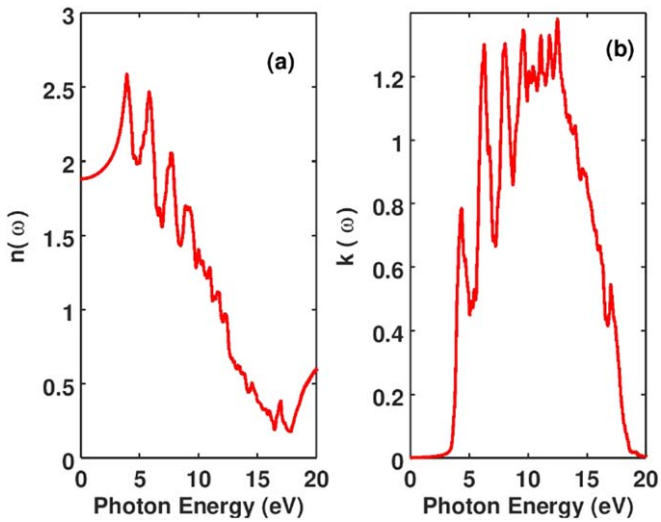

Figure 5. Calculated Refractive and Extinction Index of the SFO spinel-type.

displayed in figures 3(a) and (b). For example, the first peak is due to the transition of the electrons from the Fe-3d state in the CB to the Si-2p state in the VB. Equally, the second and third peaks are due to the electrons transition from the Fe-3d state to the Fe-3d and O-2p states. Some of the values of the energies at the different peaks of the $\varepsilon_2(\omega)$ spectra and the corresponding peak value of the $\varepsilon_2(\omega)$ are enumerated in table 3. The optical complex refractive index, $n^*(\omega)$ which is given by $n^*(\omega) = n(\omega) + ik(\omega)$ where the ordinary refractive index and the extinction coefficient are represented by $n(\omega)$ and $k(\omega)$ respectively (1).

These optical parameters are important in the design of transparent conducting oxides (TCOs) devices (1). We can clearly observe from the plot of frequency-dependent refractive index, $n(\omega)$ in figure 5(a) that, its magnitude gradually rises with energy from the zero energy ($\hbar\omega = 0,\ \lambda = \infty$) depicted value 1.88 and reach its highest value ($n(\omega)$ maximum) 6.51 corresponding to photon energy of about 4.36 eV. It is observed that the values obtained for $n(\omega)$ and that of $\varepsilon_1(\omega)$ at $\omega = 0$ obey the following relationship of $n(0) = (\varepsilon_1(0))^{1/2}$. The value obtained for the refractive of SFO spinel-type material with inclusion of the electron-hole effect is slightly higher than that of silica glass (1.45) but similar to other members of compounds (1.72) that exist in spinel form. The variation of the $k(\omega)$ (extinction coefficient) with the photon energy is exhibited in figure 5(b). The threshold energy was found to be 3,21 eV, beyond this value the $k(\omega)$ gradually increases to a maximum value of 1.42 at an energy value of 12.62 eV. The values of the different peaks of in the plot indicate that the maximum behavior of this material where further increase in the energy brings a considerable decrease in the magnitude of the extinction coefficient $k(\omega)$.

The variation of the optical conductivity ($\sigma(\omega)$) of SFO spinel-type with the photon energy is also displayed in figure 6(a). The threshold energy is 3.76 eV and above this value, the optical conductivity increases with an increase in the photon energy until it reaches a maximum value of $4.53 \times 10^{16}\ \Omega cm^{-1}$ at a photon energy of

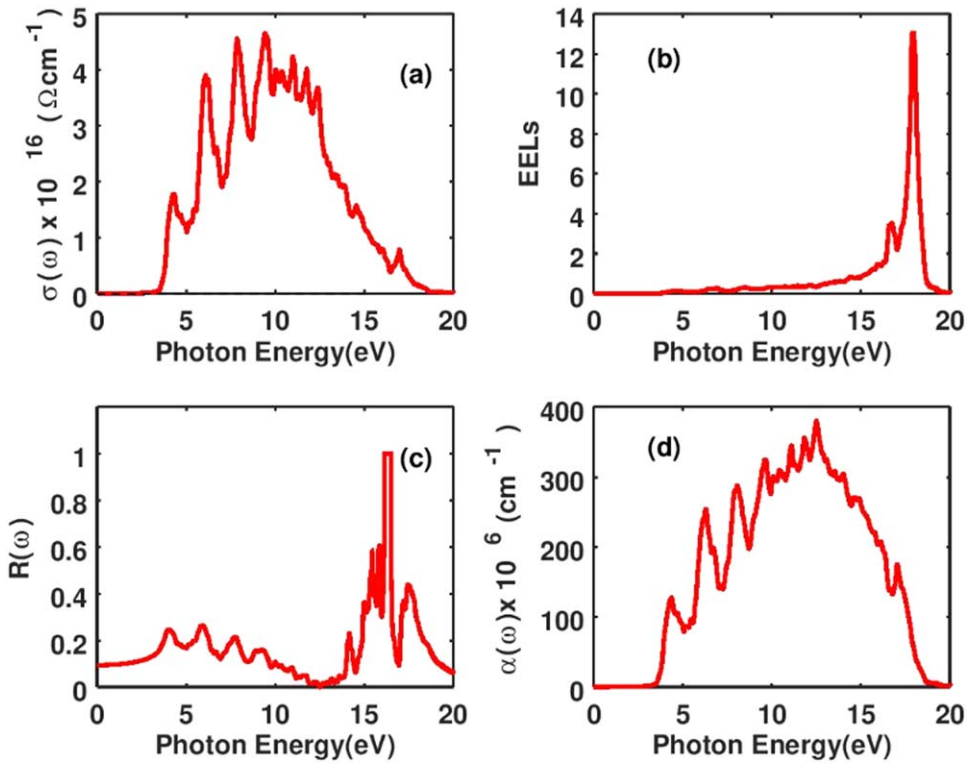

Figure 6. Calculated Conductivity, Energy Electron Loss, Reflectivity and absorption coefficient of the SFO spinel-type.

9.86 eV. Figure 6(d) displayed the optical absorption coefficient, $\propto(\omega)$ of the SFO spinel-type material. Within the energy range between 0.0 eV to 3.28 eV, the $\propto(\omega)$ is zero, and this indicates an absence of interaction between the medium and the incident photon. It was well known that this range of energy agrees that of infrared (1.24 meV to 1.7 eV) as well as that of visible (1.7 eV to 3.3 eV) region of the solar spectrum. In addition, the nonexistence of interaction between the incident photon and the material suggests that the material is transparent to the incident radiation within the 0.0 eV to 3.28 eV range. Beyond this photons energy range, the magnitude of the optical absorption coefficient starts to increase and this shows an interaction between atomic charge and photons in the medium, therefore, photons are absorbed in the medium, in figure 6(b) we can note that the $\propto(\omega)$ reaches its maximum value of 380.8 $\times$ 10^6 cm^{-1} corresponding to photon energy of about 12.25 eV. similarly, this energy range lies within the UV range of the solar spectrum thus predicts that the medium absorbs maximum photons in the UV region. Therefore, the transparency for the visible region of solar spectrum and absorbance of photons in the UV region make SFO spinel-type material useful in some devices that employ the use of TCOs such as flat panel displays and window layers in solar cells. Importantly, we observed from our calculation that there is a consistent trend for the threshold energies corresponding to $\varepsilon_2(\omega)$, $\sigma(\omega)$ and $\propto(\omega)$ spectra.

The calculated real ($\varepsilon_1(\omega)$)and imaginary ($\varepsilon_2(\omega)$) part of the complex dielectric function ($\varepsilon(\omega)$) and the various optical parameters (k(ω), n(ω), R(ω). $\propto(\omega)$ and $\sigma(\omega)$) investigated the SFO spinel-type material with the better k-points mesh within a photon energy range of 0.0 eV $-$ 20 eV did not result in any noticeable change in the trends or magnitude when compared with the spectra of various optical properties displayed in figures 5(a) and (b), as well as 6 (a, b, c and d) for the studied material and this, confirms the reliability and convergence of the computed optical properties of the material studied.

4. Conclusion

In summary, we have explored the electronic, structural and optical properties of SFO spinel-type material using first-principles pseudopotential method based on DFT + U. The investigated electronic bandstructure reveals that the SFO spinel-type material is a direct bandgap semiconductor material. We found the band gap value in this work to be 2.96 eV and 3.52 eV using LDA + U and GGA + U respectively as compared to other experimental results 4,22 eV. However, we found that the bandgap calculated with GGA + U is close to experimental value when compared to that of LDA + U. From the plots of the TDOS and PDOS, it is found that the top of the VB is mainly formed by Fe-3d and O-2p state. Also, the optical nature of SFO spinel-type material

is exposed with the help of calculating optical parameters such as complex dielectric function, index of refraction, absorption coefficient, energy loss function, reflectivity and extinction index for radiation up to 20.0 eV. The computed static complex dielectric constants have the value 6.52 and 5.42 of $\varepsilon_1(\omega)$ and $\varepsilon_2(\omega)$ respectively. Our results suggest that SFO spinel-type material is a potential candidate for some optoelectronics materials.

Acknowledgments

The authors would like to thank the Department of Physics, Universiti Teknologi Malaysia and TETFund (TETF/ES/SL.UNIV/KAFIN-HAUSA/ASTD/2017) through Sule Lamido University Kafin Hausa, Jigawa State. Nigeria for providing the facilities and financial assistance.

ORCID iDs

M C Idris https://orcid.org/0000-0003-3494-5187

References

[1] Bouhemadou A *et al* 2019 Electronic, optical, elastic, thermoelectric and thermodynamic properties of the spinel oxides $ZnRh_2O_4$ and $CdRh_2O_4$ *J Alloys Compd [Internet]* **774** 299–314
[2] Bädeker K 1907 Über die elektrische Leitfähigkeit und die thermoelektrische Kraft einiger Schwermetallverbindungen *Ann Phys [Internet]* **327** 749–66
[3] Brunin G, Ricci F, Ha V-A, Rignanese G-M and Hautier G 2019 Transparent conducting materials discovery using high-throughput computing *npj Comput Mater [Internet]* **5** 63
[4] Reffas M, Bouhemadou A, Khenata R, Ouahrani T and Bin-Omran S 2010 *Ab initio* study of structural, elastic, electronic and optical properties of spinel $SnMg_2O_4$ *Phys B Condens Matter [Internet]* **405** 4079–85
[5] Dixit H *et al* 2011 Electronic structure and band gap of zinc spinel oxides beyond LDA: $ZnAl_2O_4$, $ZnGa_2O_4$ and ZnIn $_2O_4$ *New J. Phys.* **13**
[6] Stoica M and Lo C S 2014 P-type zinc oxide spinels: application to transparent conductors and spintronics *New J. Phys.* **16**
[7] Manzar A, Murtaza G, Khenata R, Muhammad S and Hayatullah 2013 Electronic band profile and optical response of spinel $MgIn_2O_4$ through modified becke—Johnson potential. Chinese *Phys. Lett.* **30** 067401
[8] van Deelen J, Illiberi A, Hovestad A, Barbu I, Klerk L and Buskens P 2012 *Transparent Conducting Materials: Overview and Recent Results.* **8470** 84700P
[9] Stoica M, Faghaninia A, Sun X and Lo C S 2014 Computational design of p-type transparent conductors for photovoltaic applications *2014 IEEE 40th Photovolt Spec Conf PVSC 2014 [Internet]* 260–5 Available from: http://ieeexplore.ieee.org/document/6924882/
[10] Fleischer K, Norton E, Mullarkey D, Caffrey D and Shvets I V 2017 Quantifying the performance of P-type transparent conducting oxides by experimental methods *Materials (Basel) [Internet].* **10** 1–14
[11] Afre R A, Sharma N, Sharon M and Sharon M 2018 Transparent conducting oxide films for various applications: A review *Rev Adv Mater Sci.* **53** 79–89
[12] Guillén C and Herrero J 2011 TCO/metal/TCO structures for energy and flexible electronics *Thin Solid Films [Internet].* **520** 1–17
[13] Zhang Q, Meng Y, Yan C and Zhang L 2018 Synthesis of mesoporous Fe_2SiO_4/C nanocomposites and evaluation of their performance as materials for lithium-ion battery anodes *ChemistrySelect.* **3** 11902–7
[14] Dwivedi S, Sharma R and Sharma Y 2014 Electroconductive properties in doped spinel oxides *Opt Mater (Amst) [Internet].* **37** 656–65
[15] Yousaf M, Mahmood Q, Hassan M, Rashid M and Laref A 2018 *Ab initio* study of electronic, magnetic, and thermoelectric response of ZTi2O4(Z = Mg, Zn, and Cd) through mBJ potential *J. Supercond. Nov. Magn.* **4** 1–9
[16] Pinto R G, Yaremchenko A A, Baptista M F, Tarelho L A C and Frade J 2019 Synthetic fayalite Fe_2SiO_4 by kinetically controlled reaction between hematite and silicon carbide *J. Am. Ceram. Soc.* **102** 5090–102
[17] Hou Y H *et al* 2010 Structural, electronic and magnetic properties of partially inverse spinel $CoFe_2O_4$: a first-principles study *J Phys D Appl Phys [Internet].* **43** 445003
[18] Sinha M M and Kaur H 2016 Study of lattice dynamics of Fe_2SiO_4- and Mg_2SiO_4-spinels *J. Phys. Conf. Ser.* **759** 012046
[19] Davoisne C and Leroux H 2006 Structural and compositional modifications of fayalite Fe 2SiO4 under electron irradiation *Nucl Instruments Methods Phys Res Sect B Beam Interact with Mater Atoms.* **243** 371–6
[20] Wang Z *et al* 2018 Study on formation mechanism of fayalite (Fe_2SiO_4) by Solid State Reaction in Sintering Process *Jom [Internet].* **70** 539–46
[21] Ma C *et al* 2016 Ahrensite, γ-Fe_2SiO_4, a new shock-metamorphic mineral from the Tissint meteorite: Implications for the Tissint shock event on Mars *Geochim Cosmochim Acta [Internet].* **184** 240–56
[22] Xiao L, Li X and Yang X 2018 Electronic and optical properties of Fe_2SiO_4 under pressure effect: *ab initio* study *Eur Phys J B [Internet]* **91** 85
[23] Idris M C, Shaari A, Razali R, Lawal A and Ahams S T 2020 DFT + U studies of structure and optoelectronic Properties of Fe_2SiO_4 Spinel *Comput Condens Matter [Internet]* **23** e00460
[24] Rabe K M 2010 First-principles calculations of complex metal-oxide materials *Annu Rev Condens Matter Phys [Internet]* **1** 211–35
[25] Timrov I, Marzari N and Cococcioni M 2018 Hubbard parameters from density-functional perturbation theory *Phys Rev B [Internet]* **98** 085127
[26] Ono S, Kikegawa T and Higo Y 2013 *In situ* observation of a phase transition in Fe2SiO4 at high pressure and high temperature *Phys Chem Miner [Internet]* **40** 811–6
[27] Zhang J S, Hu Y, Shelton H, Kung J and Dera P 2017 Single-crystal x-ray diffraction study of Fe2SiO4 fayalite up to 31 GPa *Phys. Chem. Miner.* **44** 171–9

[28] Giannozzi P *et al* 2009 QUANTUM ESPRESSO: a modular and open-source software project for quantum simulations of materials *J Phys Condens Matter [Internet]* **21** 395502
[29] Perdew J P, Burke K and Ernzerhof M 1996 Generalized gradient approximation made simple *Phys Rev Lett [Internet]* **77** 3865–8
[30] Perdew J P and Zunger A 1981 Self-interaction correction to density-functional approximations for many-electron systems *Phys. Rev. B* **23** 5048–79
[31] Jain A *et al* 2013 Commentary: the materials project: a materials genome approach to accelerating materials innovation *APL Mater [Internet]* **1** 011002
[32] Pack H J M and J D 1976 Special points for Brillonin-zone integrations *Phys. Rev. B* **13** 1748–9
[33] Setyawan W and Curtarolo S 2010 High-throughput electronic band structure calculations: Challenges and tools *Comput Mater Sci [Internet]* **49** 299–312
[34] Murnaghan F D 1944 The compressibility of media under extreme pressure *Physics (College Park Md)* **30** 244–7
[35] Marini A, Hogan C, Grüning M and Varsano D 2009 yambo: an *ab initio* tool for excited state calculations *Comput Phys Commun [Internet]* **180** 1392–403
[36] Patrick C E and Giustino F 2012 GW quasiparticle bandgaps of anatase TiO_2 starting from DFT + U *J Phys Condens Matter [Internet]* **24** 202201
[37] Ahmad F, Agusta M K and Dipojono H K 2016 Electronic and optical properties of CuO based on DFT + U and GW approximation *J Phys Conf Ser [Internet]* **739** 012040
[38] Yu P Y and Cardona M 2010 Fundamentals of semiconductors [Internet] 4th ed.*Anesthesia and Analgesia* (Berlin, Heidelberg: Springer Berlin Heidelberg) 59, pp. 442–3 (Graduate Texts in Physics). Available from:
[39] Lawal A, Shaari A, Ahmed R and Jarkoni N 2017 Sb_2Te_3 crystal a potential absorber material for broadband photodetector: a first-principles study *Results Phys [Internet]* **7** 2302–10
[40] Woodland A B, Angel R J, Koch M, Kunz M and Miletich R 1999 Equations of state for Fe 3 2 + Fe 2 3 + Si 3 O 12 'skiagite' garnet and Fe_2SiO_4-Fe $_3O_4$ spinel solid solutions *J Geophys Res Solid Earth [Internet]* **104** 20049–58
[41] Smith H G and Langer K 1982 Single crystal spectra of olivines in the range 40,000-5000 cm-1at pressures up to 200 kbar *Am. Mineral.* **67** 347–8
[42] Burns R G 1970 Crystal field spectra and evidence of cation ordering in olivine minerals *Am. Mineral.* **9** 1608–32
[43] Zhang C-Y Y, Wang X-B B, Zhao X-F F, Chen X-R R, Yu Y and Tian X-F F 2017 First-principles calculations of structure and elasticity of hydrous fayalite under high pressure *Chinese Phys B [Internet]* **26** 126103
[44] Stackhouse S, Stixrude L and Karki B B 2010 Determination of the high-pressure properties of fayalite from first-principles calculations *Earth Planet Sci Lett [Internet]* **289** 449–56
[45] Lawal A, Shaari A, Ahmed R and Jarkoni N 2017 First-principles investigations of electron-hole inclusion effects on optoelectronic properties of Bi_2Te_3, a topological insulator for broadband photodetector *Phys B Condens Matter [Internet]* **520** 69–75
[46] Belabbas M, Arbouche O, Zemouli M, Benallou Y, Benchehima M and Ameri M 2018 *Ab initio* study of novel III–V nitride alloys B1-xTlxN for optoelectronic applications *Comput Condens Matter [Internet]* **16** e00309